Supplementary Information

In-situ conversion of delithiated residues into $Na_4Fe_3(PO_4)_2P_2O_7$ towards upcycling of spent lithium-ion batteries

Yunlong Xie[a,b,c], Wen Liu[a,b,c], Xinrong Deng[a,b,c], Jie Zhou[a,b,c], Danlin Ouyang[a,b,c], Binod Mahara[a,b,c], Lishan Yang[a,b,c*], Xiangping Chen[a,b,c*], Yong Pei[a,d]

[a] *College of Chemistry and Chemical Engineering, Hunan Normal University, Changsha, Hunan Province 410081, P.R. China;*

[b] *National and Local Joint Engineering Laboratory for New Petrochemical Materials and Fine Utilization of Resources, Hunan Normal University, Changsha 410081, P.R. China;*

[c] *Key Laboratory of the Assembly and Application of Organic Functional Molecules of Hunan Province, Key Laboratory of Light Energy Conversion Materials of Hunan Province, Hunan Normal University, Changsha 410081, P.R. China;*

[d] *Department of Chemistry, Key Laboratory of Environmentally Friendly Chemistry and Applications of Ministry of Education, Key Laboratory for Green Organic Synthesis and Application of Hunan Province, Xiangtan University, Hunan Province 411105, China.*

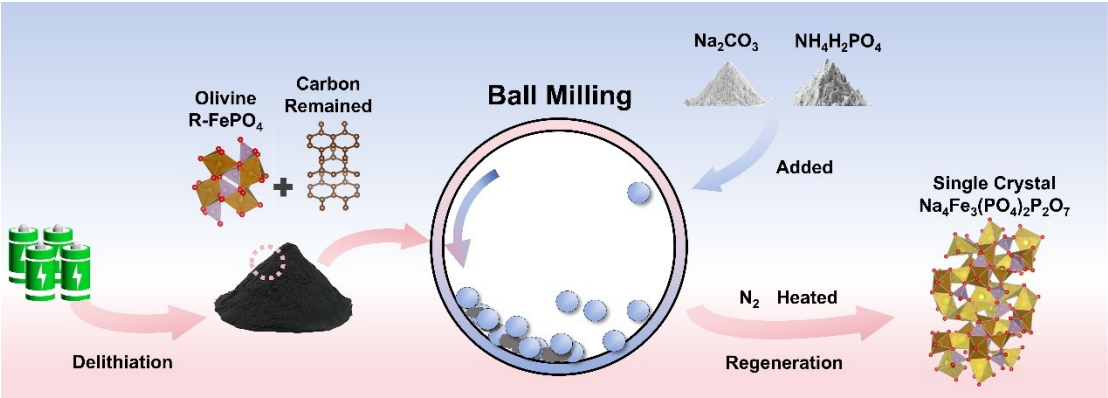

Fig. S1. Schematic diagram of the experimental process.

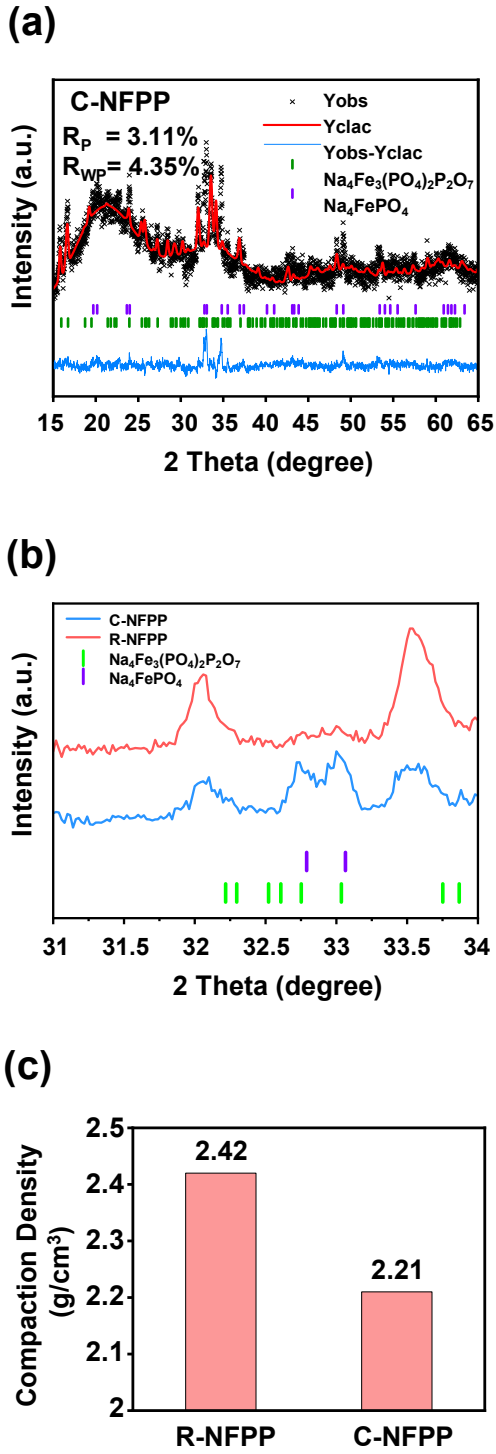

Fig. S2. (a) The rietveld refinement profiles of C-NFPP from SXRD patterns. (b) XRD comparison of local parts between C-NFPP and R-NFPP. (c) The compaction density of C-NFPP and R-NFPP.

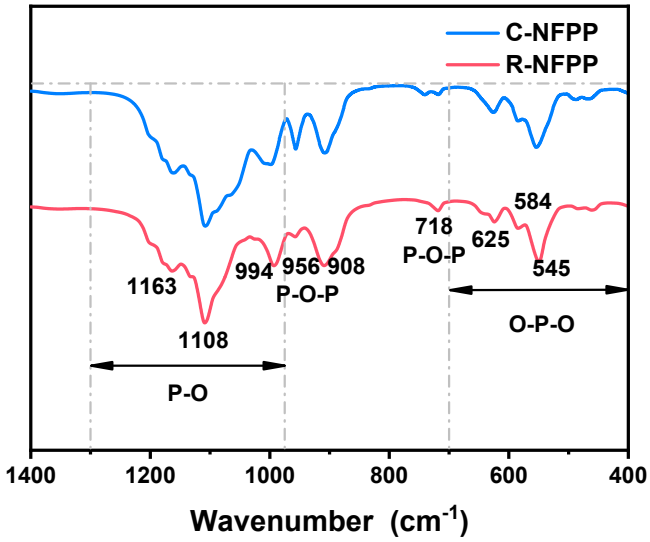

Fig. S3. Fourier transform infrared (FT-IR) spectra of C-NFPP and R-NFPP.

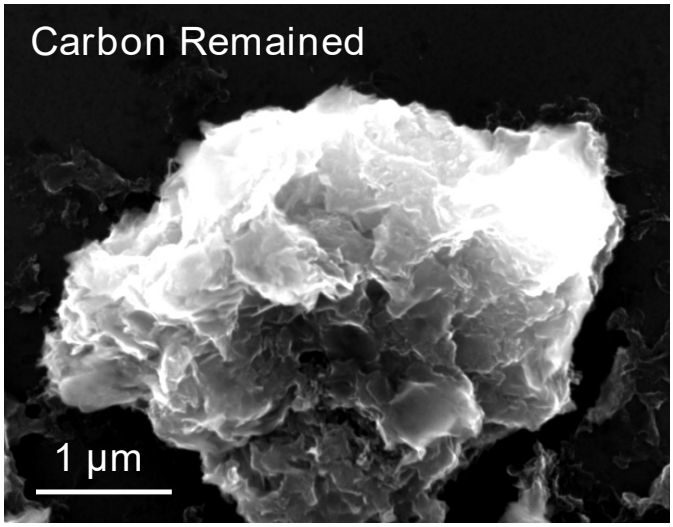

Fig. S4. The SEM image of Carbon Remained.

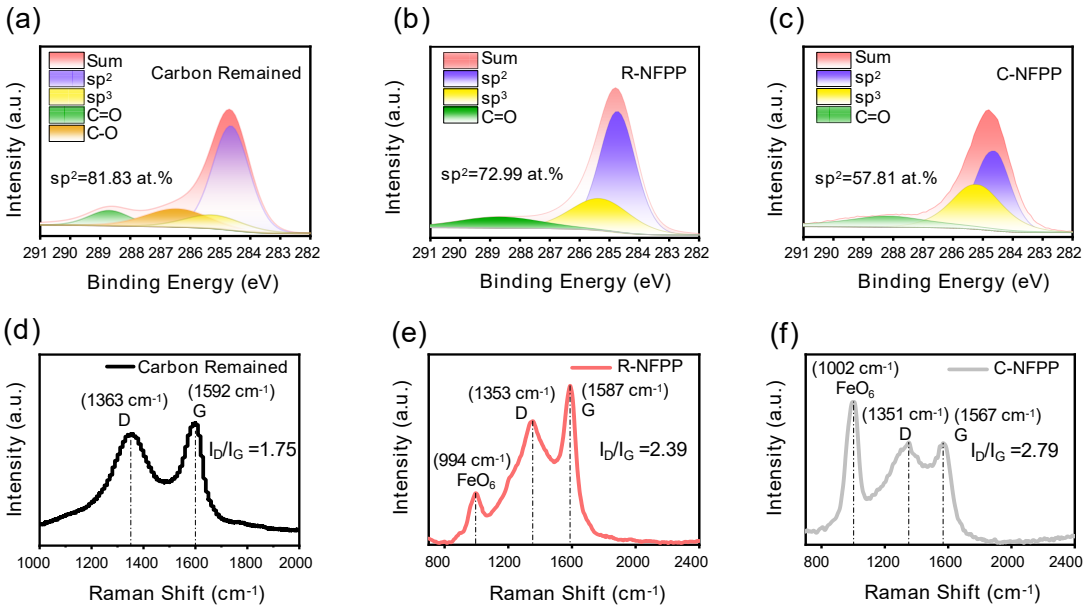

Fig. S5. Carbon coating analysis. The XPS spectra of C 1s of (a) Carbon Remained, (b) R-NFPP and (c) C-NFPP.

The Raman spectra of (d) Carbon Remained, (e) R-NFPP and (f) C-NFPP.

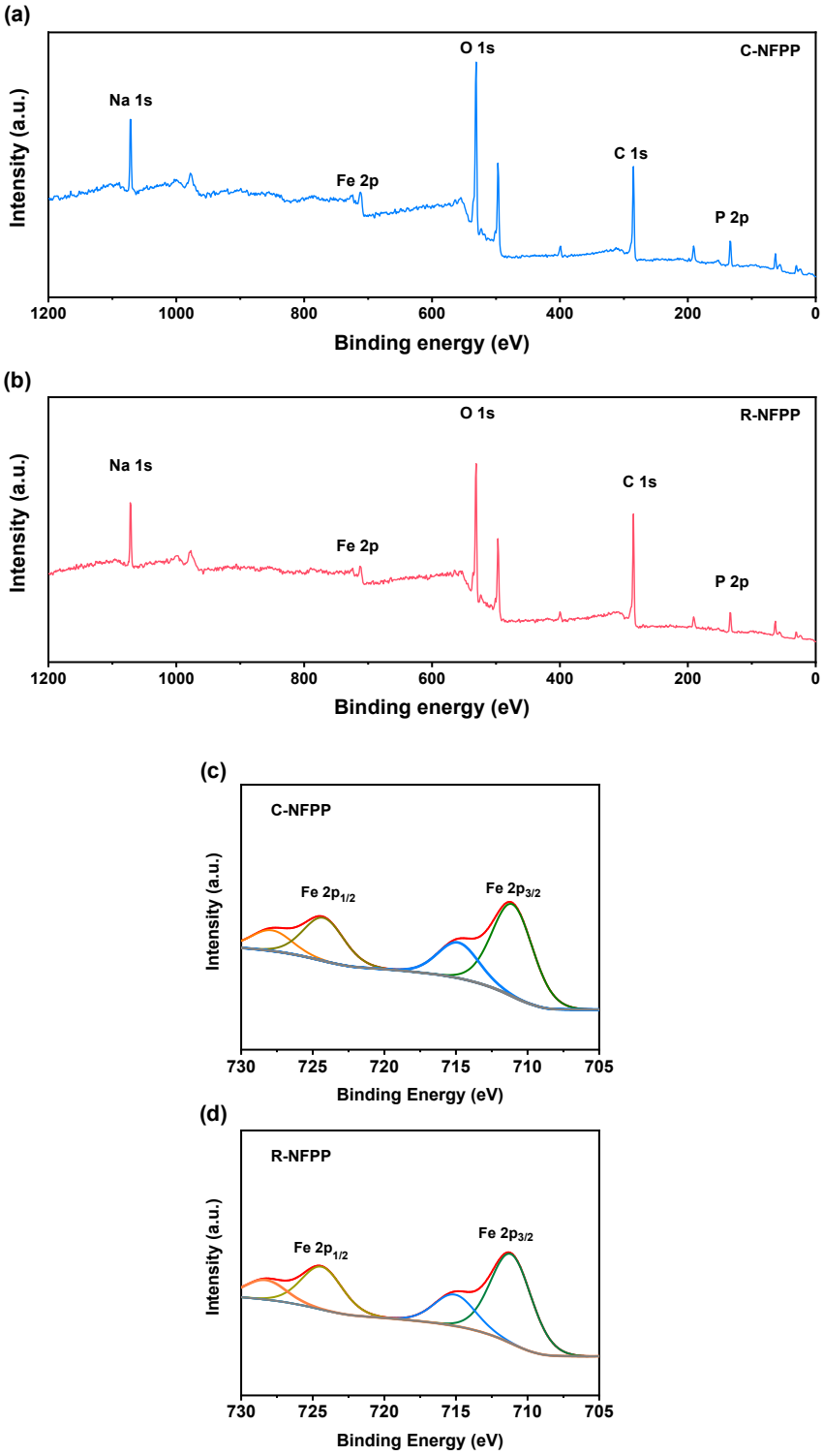

Fig. S6. XPS spectra of survey (a, c) and Fe 2p (b, d) in C-NFPP and R-NFPP.

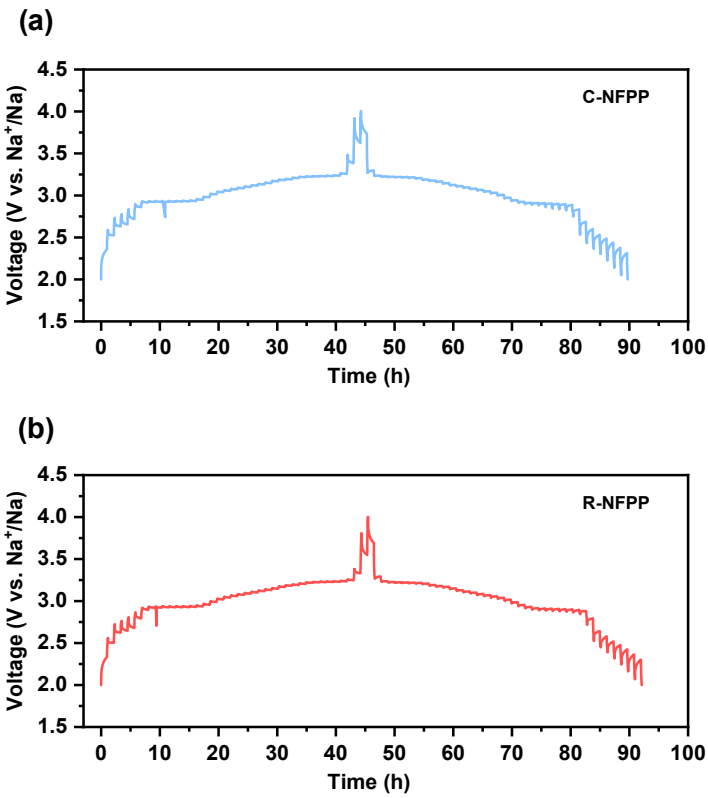

Fig. S7. GITT curves of C-NFPP (a) and R-NFPP (b).

The equation for D_{Na^+} is as follows:

$$D_{Na^+}=(4L^2/\pi\tau)(\Delta E_s/\Delta E_\tau)^2 \quad (\tau \ll L^2/D_{Na^+})$$

where L is the effective thickness of the electrode material, τ is the pulse time, π is 3.15, ΔE_s is the open circuit potential difference between two adjacent pulse, and ΔE_τ is the change of potential caused by an impulse.

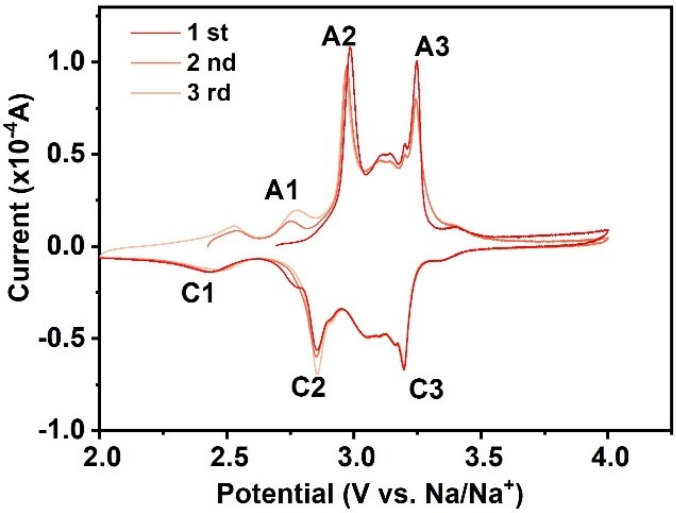

Fig. S8. CV of C-NFPP between 2 and 4 V in the first three laps.

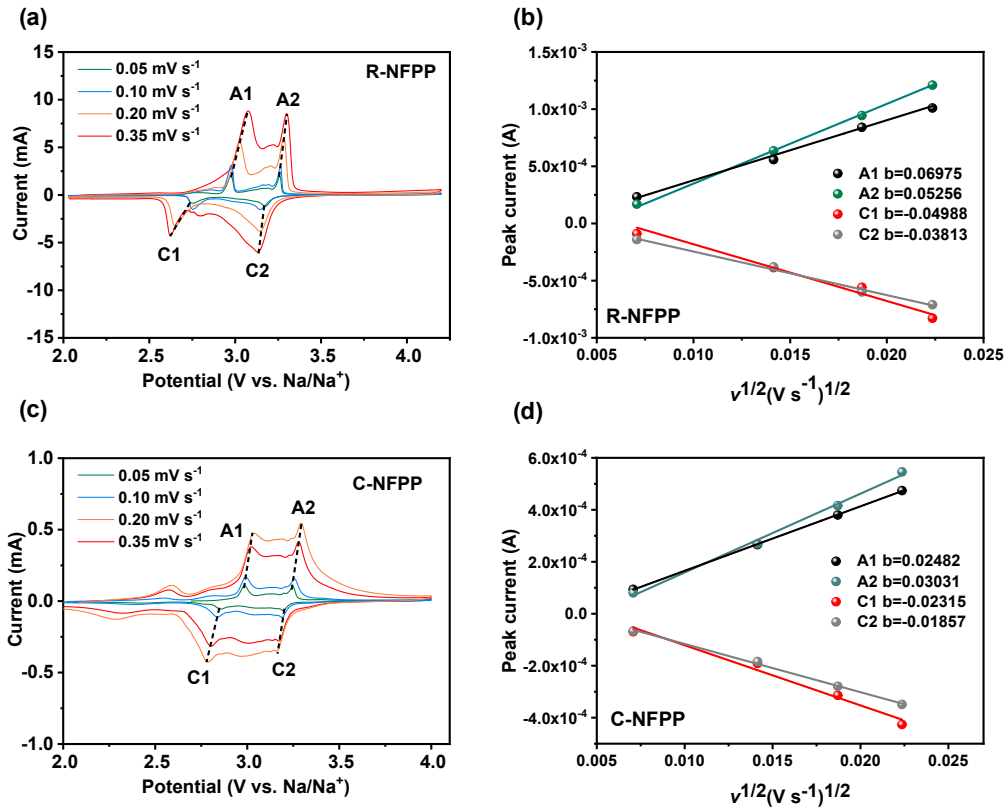

Fig. S9. (a, c) CV curves at various scan rates from 0.1 to 1.0 mV s^{-1}, of C-NFPP and R-NFPP cathodes, and corresponding (b, d) linear relationships between the square root of scan rate ($v^{1/2}$) and the peak current (i_p)

As shown in **Figure S9**, the peak currents (i_a, i_c) exhibit a linear relationship with the square root of the scan rate ($v^{1/2}$), suggesting that the Na^+ ion storage mechanism in NFPP is predominantly diffusion-controlled at low current rates. The sodium ion diffusion coefficient within the bulk material can be calculated using the Randles-Sevcik equation:

$$I_p=2.69 \times 10^5 n^{3/2} A D^{1/2} C_0 v^{1/2}$$

Where i_p represents the peak current (A), n is the number of electrons transferred per species in the reaction (n=3 in this system), A is the contact area between the working electrode and electrolyte (1.54 cm^2), D_{Na^+} is the diffusion coefficient of sodium ions (cm^2 s^{-1}), C_0 is the bulk concentration of sodium ions in the electrode (5.04×10^{-3} mol

cm^{-3}), and v is the scan rate ($mV\ s^{-1}$). Based on the linear relationships fitted between i_p and $v^{1/2}$, the D_{Na^+} values for R-NFPP are calculated as $4.73 \times 10^{-11}\ cm^2\ s^{-1}$ (Peak A1), $2.68 \times 10^{-11}\ cm^2\ s^{-1}$ (Peak A2), $2.42 \times 10^{-11}\ cm^2\ s^{-1}$ (Peak C1), and $1.41 \times 10^{-11}\ cm^2\ s^{-1}$ (Peak C2). Similarly, the D_{Na} values for C-NFPP are $5.99 \times 10^{-12}\ cm^2\ s^{-1}$ (Peak A1), $8.93 \times 10^{-12}\ cm^2\ s^{-1}$ (Peak A2), $5.21 \times 10^{-12}\ cm^2\ s^{-1}$ (Peak C1), and $3.35 \times 10^{-12}\ cm^2\ s^{-1}$ (Peak C2).

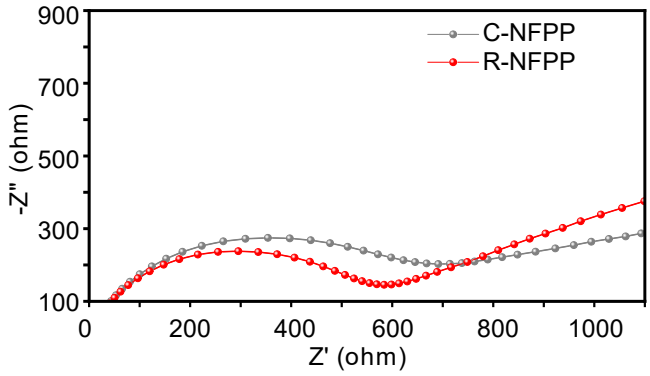

Figure S10. EIS spectra of C-NFPP and R-NFPP cells.

Fig. S10. displays the Nyquist plots, which consist of a semicircle in the high-to-medium frequency region and a sloping line in the low-frequency region. The semicircle corresponds to the charge-transfer resistance (R_{ct}) at the electrode/electrolyte interface, while the sloping line represents the Warburg impedance (Z_w), associated with Na^+ diffusion within the electrode. The R_{ct} values were determined by fitting the curves using the equivalent circuit shown in the inset of Fig. 5a. The Rct of the R-NFPP sample (598.3 Ω) is significantly lower than that of C-NFPP (692.4 Ω). Electrochemical impedance spectroscopy (EIS) is also a powerful tool for evaluating the Na^+ diffusion coefficient (D_{Na^+}). The diffusion kinetics can be calculated using the following equations:

$$\sigma = RT/(An^2F^2C\,(2D_{Na^+})^{1/2})$$

$$Z' = R_s + R_{ct} + \sigma\omega^{-1/2}$$

Where R is the gas constant (8.314 J mol^{-1} K^{-1}), T is the absolute temperature (298 K), A is the electrode/electrolyte contact area (1.54 cm^2), n is the number of transferred electrons (n=3 in this system), F is the Faraday constant (96500 C·mol^{-1}), C is the Na^+ concentration in the cathode (5.04×10^{-3} mol cm^{-3}), and σ is the Warburg factor. The Na^+ diffusion coefficient (D_{Na^+}) can be calculated using Equation, while σ is derived from the relationship between Z′ and $\omega^{-1/2}$. The value of σ is determined from the slope of the Z′ vs. $z^{-1/2}$ plot. As calculated, the slope of R-NFPP is much lower than that of C-NFPP, indicating a higher D_{Na^+} value.

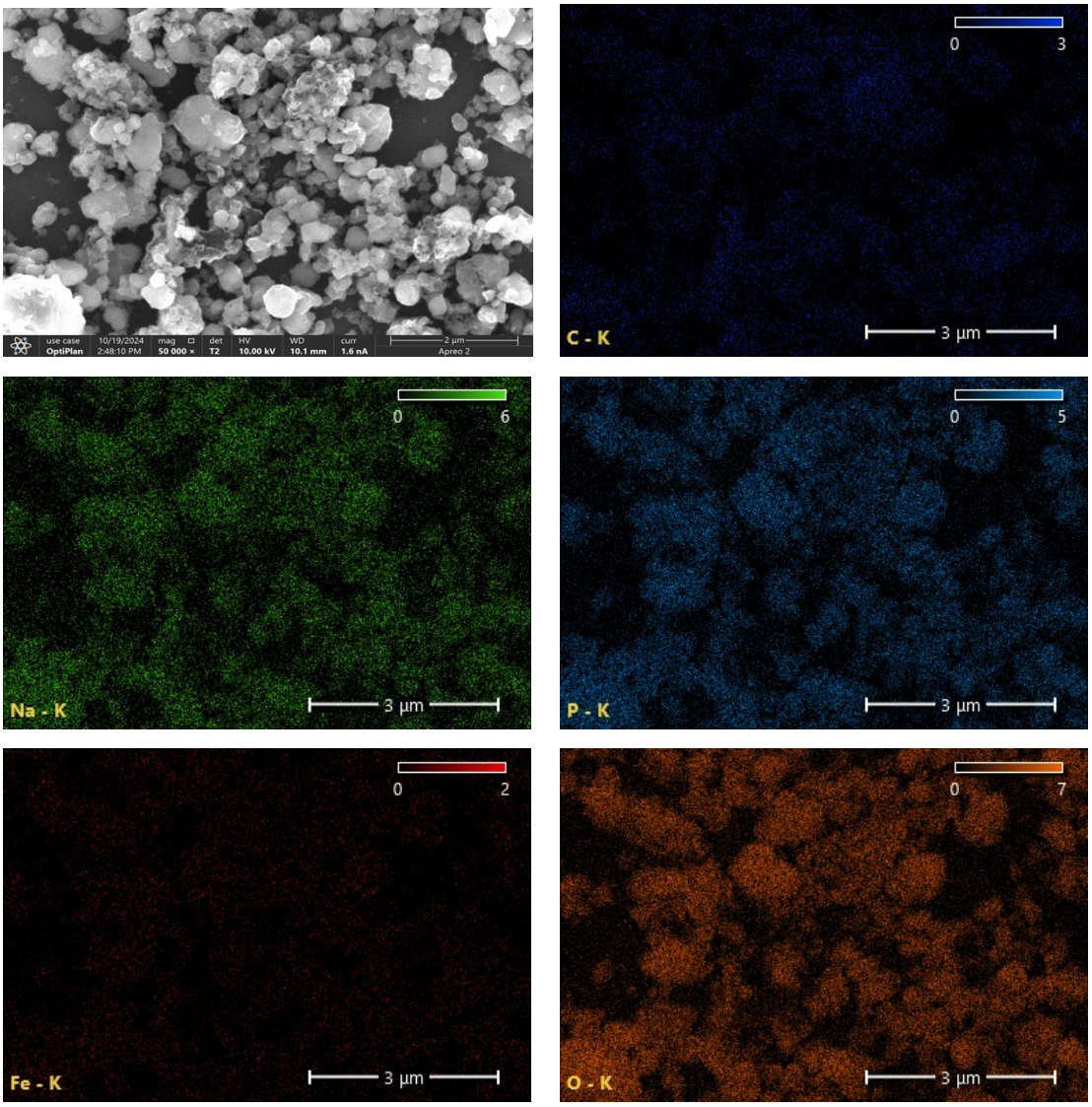

Fig. S11. SEM image of R-NFPP and the element mappings.

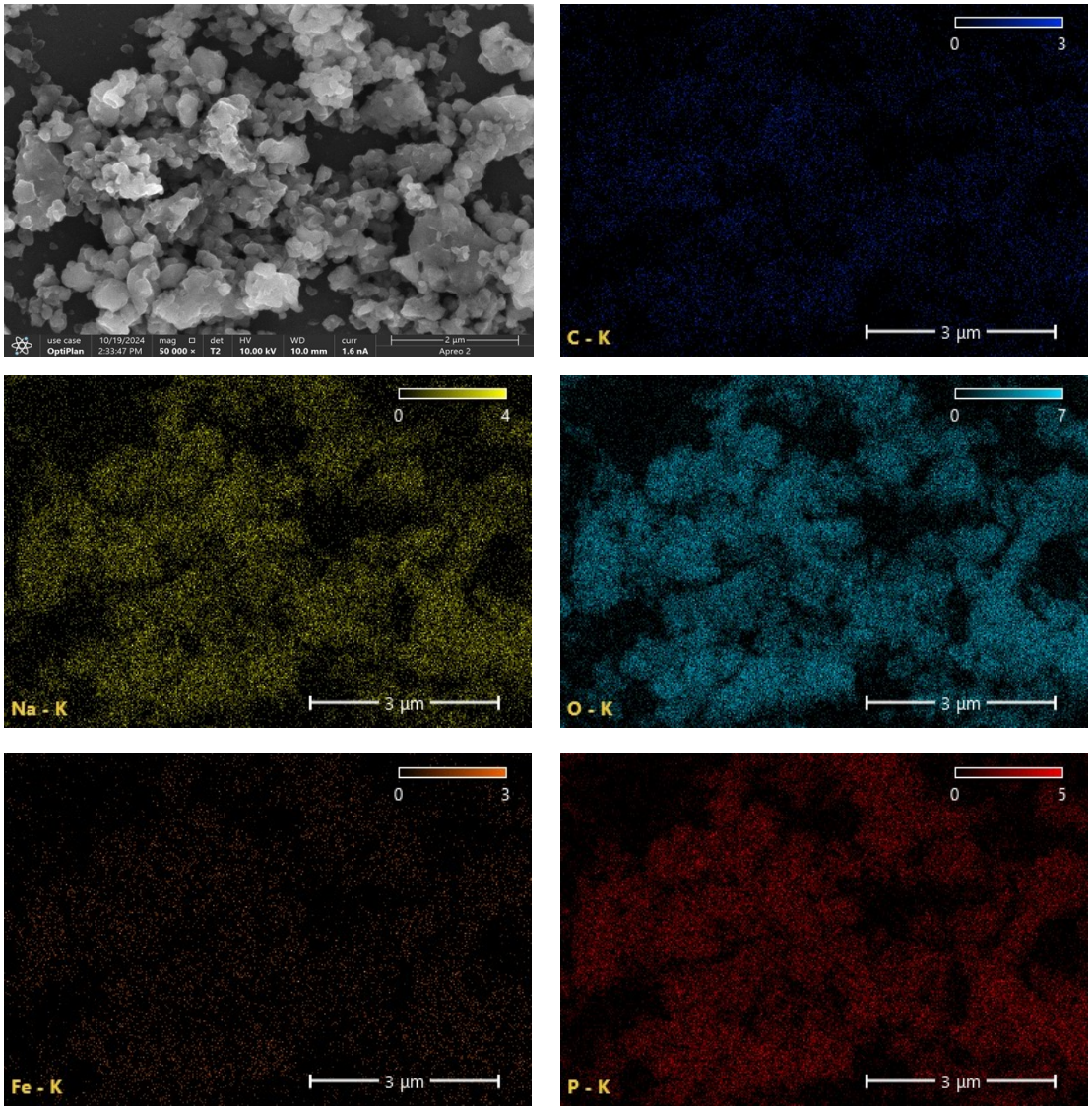

Fig. S12. SEM image of C-NFPP and the element mappings.

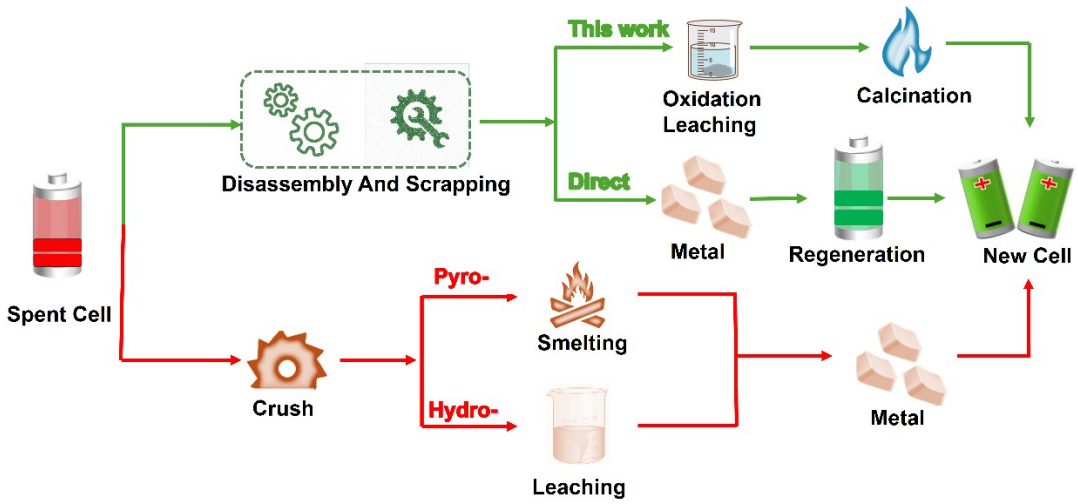

Fig. S13. Schematic diagram of the recycling economic model.

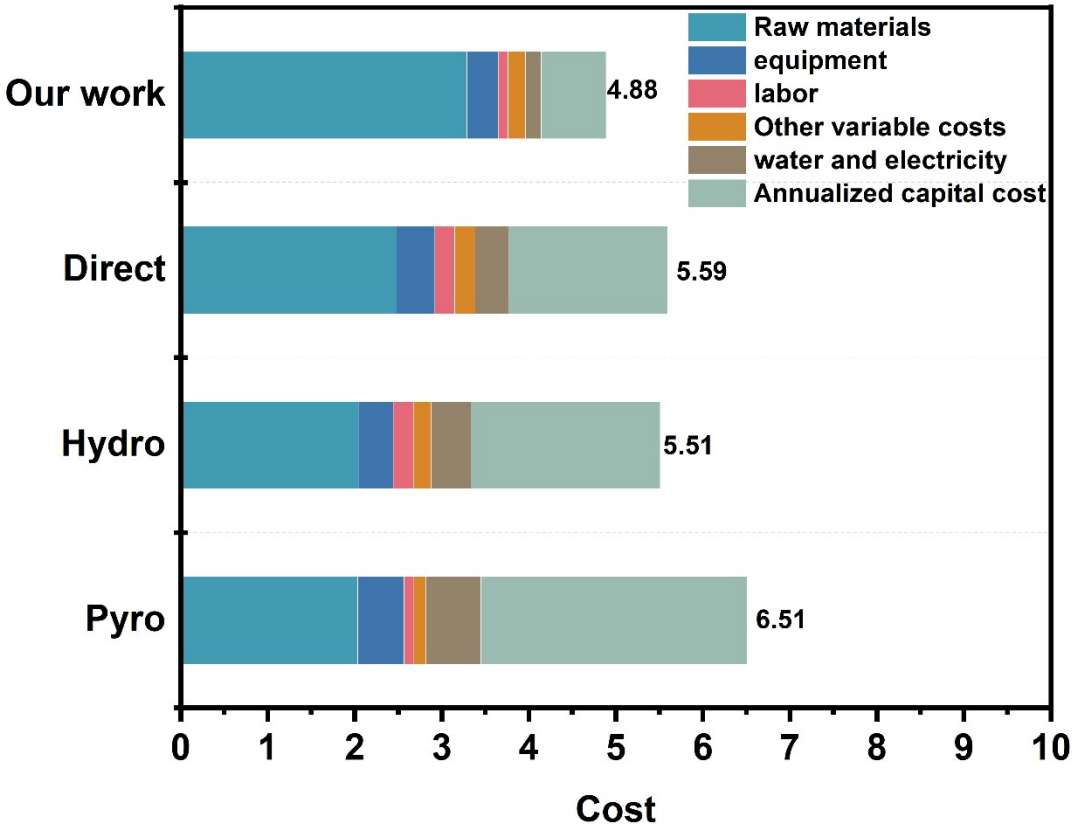

Fig. S14. Cost of the four methods.

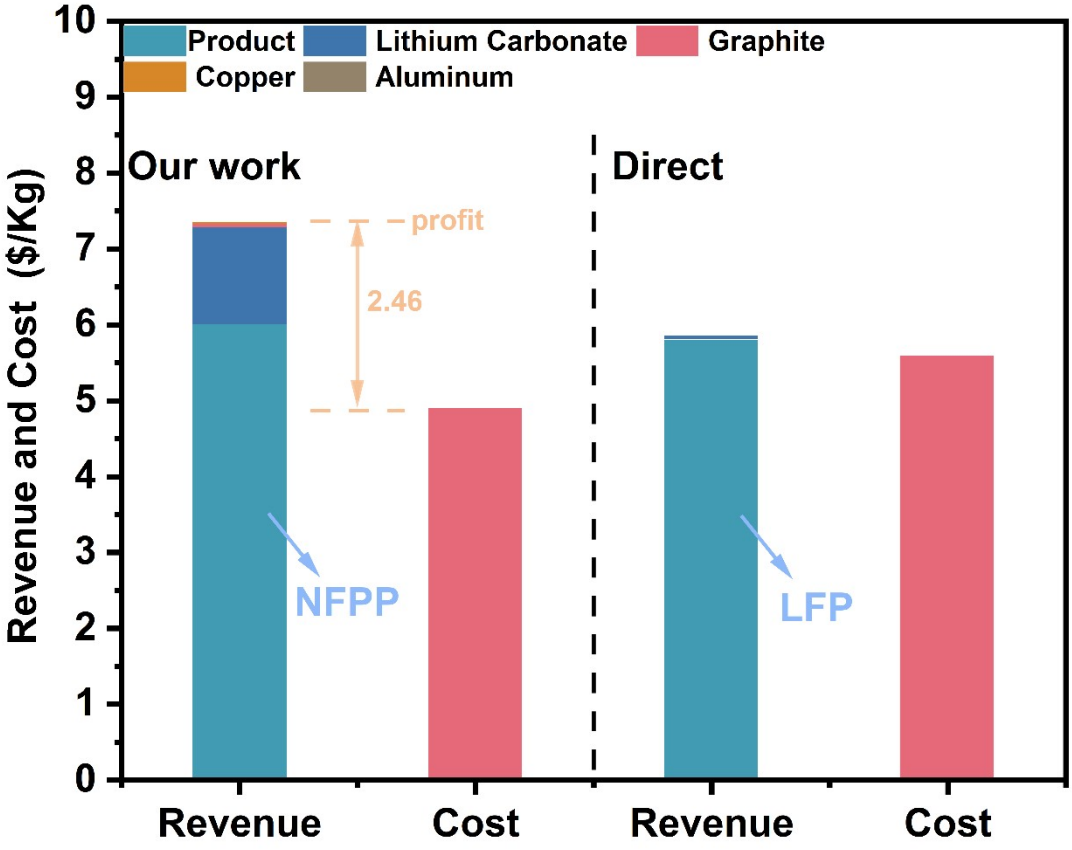

Fig. S15. Cost and revenue of this method and direct regeneration.

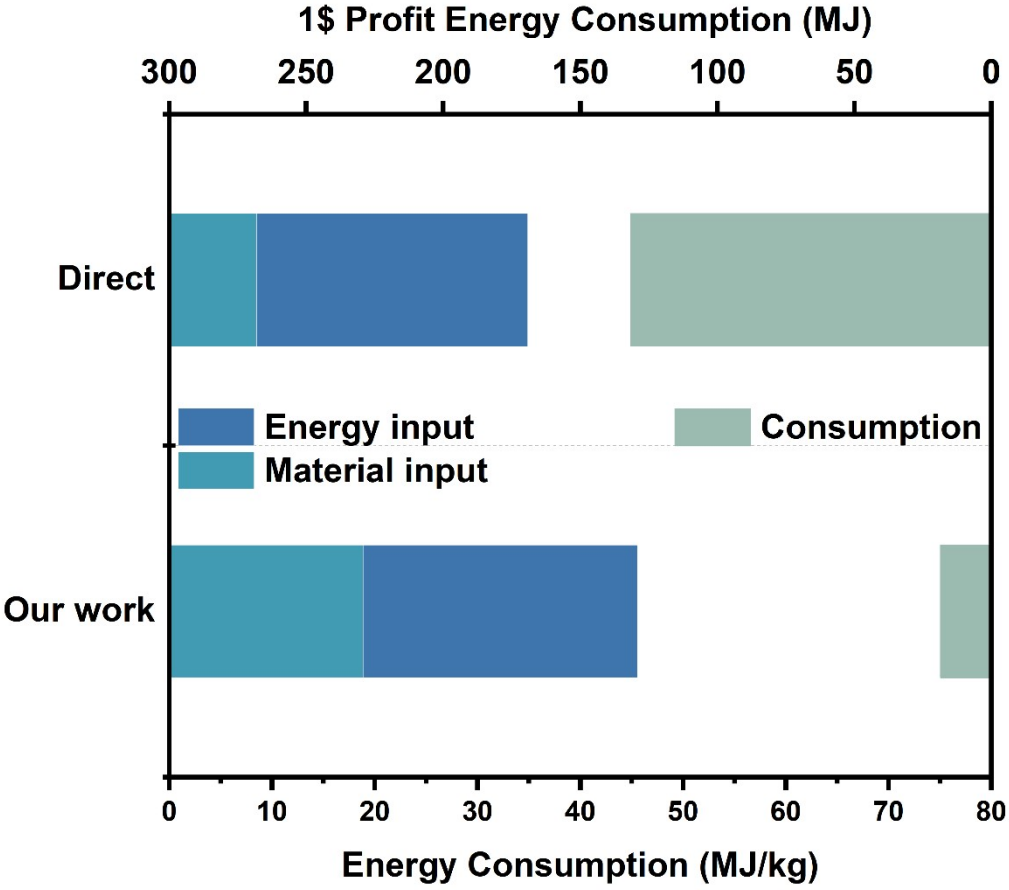

Fig. S16. Energy consumption of this method and direct regeneration.

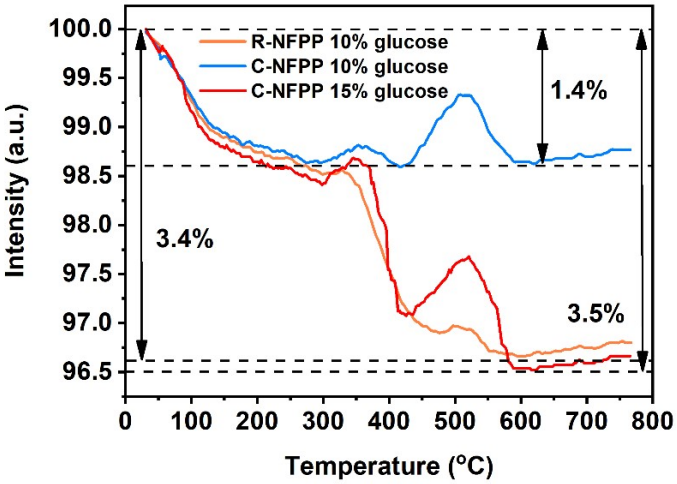

Fig. S17. Thermogravimetric analysis (TG) curves of three samples.

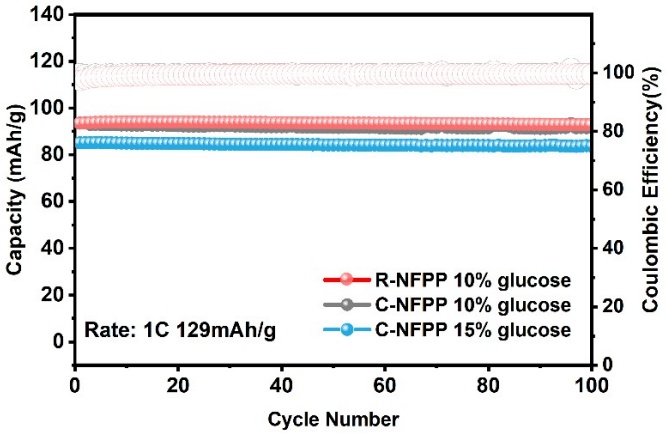

Fig. S18. Cycle stability and coulombic efficiency at 1 C

Table S1. Detailed structural information of NFPP after Rietveld determined from the Rietveld refined SXRD pattern.

Formula	C-NFPP	R-NFPP
Crystal system	Orthorhombic	Orthorhombic
Space group	$Pn2_1a$	$Pn2_1a$
Lattice parameter *a* (Å)	18.144088	18.189848
Lattice parameter *b* (Å)	10.682700	10.675031
Lattice parameter *c* (Å)	6.544132	6.521152
α	90°	90°
β	90°	90°
γ	90°	90°
Unit-cell volume ($Å^3$)	1311.444	1313.729

Table S2. Energy density performance of R-NFPP and C-NFPP under varied current densities and temperature conditions (theoretical specific capacity: 129 mAh g^{-1})

Condition	C-NFPP	R-NFPP
0.1 C	101.51 mAh g^{-1}	107.84 mAh g^{-1}
0.5 C	89.50 mAh g^{-1}	94.66 mAh g^{-1}
1 C	86.63 mAh g^{-1}	88.62 mAh g^{-1}
2 C	81.89 mAh g^{-1}	82.86 mAh g^{-1}
5 C	73.34 mAh g^{-1}	75.24 mAh g^{-1}
10 C	57.69 mAh g^{-1}	68.57 mAh g^{-1}
15 C	42.51 mAh g^{-1}	63.70 mAh g^{-1}
20 C	29.90 mAh g^{-1}	59.86 mAh g^{-1}
25 C	20.52 mAh g^{-1}	56.61 mAh g^{-1}
50 C	3.76 mAh g^{-1}	46.23 mAh g^{-1}
100 C	0.72 mAh g^{-1}	35.84 mAh g^{-1}

Table S3. Chemical compositions of the R-FPO, C-NFPP and R-NFPP measured by inductively coupled plasma analysis (ICP).

Sample	Measured atomic ratio			
	Na	Fe	P	Li
R-FPO	0	1	1	0.001
C-NFPP	4.00	3	3.99	0
R-NFPP	4.00	3	4.01	0

Table S4. The comparison of electrochemical performance of R-NFPP and other reported NFPP-based cathode materials in coin cell. The negative electrode is Na disc and the operated at room temperature.

Materials	Cycle performance Capacity retention/cycle number/current density (mA g^{-1})	Rate performance Capacity (mAh g^{-1})/current density (mA g^{-1})	Ref.
NFPP/C nanoparticles	89%/300/64.5	99/25.8, 97/64.5, 95/129, 92/258, 86/645, 78/1290	1
3D graphene decorated NFPP microspheres#	62.3%/6000/1290	117.4/12.9, 111.9/25.8, 107.3/64.5, 104.5/129, 102.7/258, 96.3/645, 92.6/1290, 85.3/2580, 69.7/6450, 55/12900, 32.1/25800	2
NFPP@$NaFePO_4$@C on carbon cloth	>100%/3,000/1290 ~90%/3,000/6450	127/64.5, 118/129, 113/258, 104/645, 97/1290, 89/2580, 75/6450, 68/12900	3
NFPP/C nanospheres#	63.5%/4000/1290	108.2/25.8,105.2/64.5, 102.4/129, 101.2/258, 99.6/645, 97.4/1290, 95.5/2580, 92.3/3870, 90.4/6450, 77.9/10320, 67.7/12900	4
Nanoplate-like NFPP/C	69.1%/4400/2400	113.0/6, 108.3/12, ~105/24, ~102/60, ~100/120, ~95/360, ~89/600, ~84/1200, 80.3/2400	5

Table S5. The comparison of economy of R-NFPP and other reported NFPP-based cathode materials

References	[1]	[2]	C-NFPP	R-NFPP
Method	Spray Drying	Spray Drying	Ball Milling	Ball Milling
Raw Materials	Ferrous oxalate	Ferrous oxalate	Waste $LiFePO_4$	Waste $LiFePO_4$
Cost of ion materials ($/kg)	8	8	0.5	0.5
process costs ($/kg)	Spray Drying 30	Spray Drying 30	Recycling Process 13 Ball Milling 10	Recycling Process 7 Ball Milling 10
Environmentally friendly	Low	Low	High	High
energy consumption	High	High	High	Low
economy	Low	Low	Normal	High

References

1 X. H. Wu, G. M. Zhong, Y. Yang, *J. Power Sources.*, 2016, 327, 666-674.

2 T. C. Yuan, Y. X. Wang, J. X. Zhang, X. J. Pu, X. P. Ai, Z. X. Chen, H. X. Yang, Y. L. Cao, *Nano Energy*, 2019, 56, 160-168

3 X. D. Ma, Z. Y. Pan, X. H. Wu, P. K. Shen, *Chem. Eng. J.*, 2019, 365, 132-141.

4 X. Pu, H. Wang, T. Yuan, S. Cao, S. Liu, L. Xu, H. Yang, X. Ai, Z. Chen, Y. Cao, *Energy Storage Mater.*, 2019, 22, 330-336.

5 M. Chen, W. Hua, J. Xiao, D. Cortie, W. Chen, E. Wang, Z. Hu, Q. Gu, X. Wang, S. Indris, S. L. Chou, S. X. Dou, *Nat Commun.*, 2019, 10, 1480.